JGR Atmospheres

RESEARCH ARTICLE
10.1029/2020JD034083

# Impact of a Nocturnal Low-Level Jet on Surface-Layer Turbulent Characteristics

**N. A. Brunsell**[1], **D. A. Rahn**[1], **and D. B. Mechem**[1]

[1]Department of Geography and Atmospheric Science, University of Kansas, Lawrence, KS, USA

**Key Points:**

- The Great Plains Low-Level Jet (GPLLJ) is a dominant meteorological feature in the central US
- The presence of the GPLLJ impacts surface-layer turbulence
- Some aspects of the turbulence are also impacted by the magnitude of the low-level jet

**Correspondence to:**
N. A. Brunsell,
brunsell@ku.edu

**Citation:**
Brunsell, N. A., Rahn, D. A., & Mechem, D. B. (2021). Impact of a nocturnal low-level jet on surface-layer turbulent characteristics. *Journal of Geophysical Research: Atmospheres*, *126*, e2020JD034083. https://doi.org/10.1029/2020JD034083

Received 12 OCT 2020
Accepted 16 MAR 2021

**Author Contributions:**
**Conceptualization:** N. A. Brunsell
**Formal analysis:** N. A. Brunsell
**Methodology:** N. A. Brunsell
**Visualization:** N. A. Brunsell
**Writing – original draft:** N. A. Brunsell

**Abstract** The impact of the Great Plains Low-Level Jet (GPLLJ) on the surface-layer turbulent characteristics is investigated using a long-term data set of eddy-covariance observations. The presence of the GPLLJ alters the distribution of the normalized wind velocity standard deviations and the turbulent intensity. Spectral analysis indicates that the presence of the GPLLJ can alter the low-frequency contribution in the *u*-spectra as well as the anisotropy of the *u* and *w* components of the flow. The intensity of the LLJ impacts the high-frequency contributions to the *w*-spectra. Using quadrant analysis to examine how the LLJ impacts sweeps and ejections, we find that the presence and the intensity of the LLJ alters the correlation between *u* and *w*. In addition, the intensity of the LLJ impacts the relative contribution from different quadrants to the overall flux and also impacts the third-order moments. Therefore, the presence of the LLJ alters surface-layer turbulence, while LLJ intensity appears to impact only a subset of these factors.

## 1. Introduction

The Great Plains Low-Level Jet (GPLLJ) stretches from Texas into Nebraska with a climatological maximum over northern Oklahoma and southern Kansas (Bonner, 1968; Hoecker, 1963; Mitchell et al., 1995; Song et al., 2005). The LLJ is an integral component in the atmospheric system over Kansas and has been the focus of many studies. It transports boundary-layer moisture from the Gulf of Mexico deep into the interior of the continental United States with estimates that up to one third of the moisture flux is associated with the LLJ (Helfand & Schubert 1995; Higgins et al., 1997). Initiation and maintenance of organized convection is favored at the northern nose of the LLJ, with the resulting precipitation contributing substantially to the annual total (Tuttle & Davis, 2006). Increased wind speed associated with the LLJ is important to the production of electricity from wind farms but can also have detrimental effects due to increased vertical shear and nighttime turbulence near the wind turbine hub height, which puts more stress on the rotors (e.g., Zhang et al., 2019).

Formation of a LLJ can be tied directly to transient synoptic features such as leeside troughing or the interaction between the lee trough and an upper-level jet (Uccellini, 1980), but a LLJ often forms without these transient features. The Great Plains LLJ is common during the warm season since there is a favorable synoptic low-level pressure gradient associated with the semi-permanent Bermuda high. This sets up a background state that drives a persistent southerly flow that is frequently connected to jet events such that the mean low-level flow is referred to as the "climatological Great Plains LLJ" (Cook et al., 2008). The large-scale pressure gradient over the Great Plains is enhanced by the mean summertime heating of the sloping terrain since it establishes a mean isobaric temperature gradient that, by thermal wind arguments, enhances the horizontal pressure gradient (Bonner & Paegle, 1970). The LLJ becomes most pronounced over night when the turbulent mixing near the surface decreases and the boundary-layer decouples from the surface. Nighttime wind speeds typically peak around 15–20 $s^{-1}$ at 300–800 m above the surface. There is a lingering debate over the causes of the LLJ, but mechanisms that support its formation include an inertial oscillation (Blackadar, 1957; Parish & Oolman, 2010; Shibuya et al., 2014), baroclinicity associated with sloping terrain (Holton, 1967), conservation of potential vorticity (Zhong et al., 1996), and large-scale meteorological forcing (Song et al., 2005). The Great Plains LLJ is still an active area of research after decades of investigation (e.g., Gebauer & Shapiro, 2019; Jahn & Gallus, 2018; Parish & Clark, 2017; Smith et al., 2019).

Eddy-covariance observations have been used to assess the impact of the LLJ on near-surface turbulence. Prabha et al. (2007) investigated the role of the LLJ on low-frequency turbulent dynamics and found that

strong LLJ conditions were associated with a reduction in the low-frequency contributions because of extreme shear, but that moderate LLJ conditions exhibited significant low-frequency contributions and significant intermittent turbulent bursts. These low-frequency contributions were shown to result in counter-gradient fluxes (Prabha et al., 2007).

Using three months of eddy-covariance tower data, Duarte et al. (2015) showed that the presence of the LLJ usually resulted in more developed turbulence and an increase in turbulent intensity. El-Madany et al. (2014) found similar results, with the LLJ associated with increased turbulent intensity and impacting the vertical velocity spectra. Karipot et al. (2008) found that the alteration of the turbulent flow accompanying LLJ events resulted in building up and venting of $CO_2$ fluxes within a forest canopy.

Each of the above cases used only a limited amount of eddy-covariance observations (up to several months) to assess the impact of the LLJ on turbulent flow near the surface. The goal of the present work is to explore the generality of the above results by employing a long-term data set of near-surface turbulent measurements. We wish to extend the previous work by assessing the impacts of both the presence and intensity of the LLJ to further characterize to what extent the LLJ alters near-surface turbulent dynamics.

## 2. Methods

### 2.1. Eddy-Covariance Data and Processing

The Konza Prairie Ameriflux site (US-KON) is used to assess the impact of the LLJ on surface-layer turbulent characteristics. The Konza Prairie is located south of the city of Manhattan in north-central Kansas. The site is a native tallgrass prairie, burned annually, and experiences annual precipitation of 844 mm. For further details on the site and local characteristics, the reader is referred to Brunsell et al. (2014) and Logan and Brunsell (2015).

Turbulence data at the site were collected at 3 m above the surface. Three-dimensional wind components, temperature, humidity, and carbon dioxide concentration were collected at 20 Hz using a triaxial sonic anemometer (CSAT-3, Campbell Scientific, Logan UT, USA) and a Li-Cor infrared gas analyzer (LI-7500, Li-Cor, Lincoln, NE, USA). Springtime (March-May) data for 2008–2017 were used in this analysis. The LLJ is predominantly a warm season phenomenon. Springtime data was therefore chosen for the present analysis to maximize a large number of events while minimizing issues with seasonal variation in the variables of interest. Data were filtered so that only nighttime (6 p.m. to 6 a.m.) half-hour periods with 100% data were used.

Any outliers with an absolute value greater than the mean ±5 standard deviations for that half-hour period were removed. A coordinate rotation was applied to every half-hour following Kaimal and Finnigan (1994). The Obukhov length was computed from the half-hourly quantities as $L = -u_*^3\overline{T} \,/\, (kg\overline{w'T'})$ where $u_*$ is the friction velocity, $T$ is the temperature, $k$ is the von Karman constant (0.4), $g$ is the acceleration due to gravity (9.8 m $s^{-2}$), and $\overline{w'T'}$ is the kinematic heat flux.

Fourier transforms of the wind data were calculated for every half-hour period that exhibited statically stable conditions ($z/L > 0$, where $z$ is the tower height). Linear trends are removed and a Welch window is applied to the ends of the data prior to the Fourier transform. The half-hourly spectra are normalized by the frequency and mean horizontal ($\overline{U}$) wind speed to facilitate comparison across time periods with different flow characteristics. The normalized spectra are then averaged by LLJ criteria (explained below) by bin averaging in the normalized frequency range. In addition, the spectra presented here are smoothed in log space to facilitate visualization.

### 2.2. Quadrant Analysis

Quadrant analysis is used to determine to what extent the LLJ alters the characteristics of the surface-layer flow. We follow the analysis and techniques outlined in Katul et al. (1997). We define the quadrants as Q1: $u' > 0$; $w' > 0$, Q2: $u' > 0$; $w' < 0$, Q3: $u' < 0$; $w' < 0$, Q4: $u' < 0$; $w' > 0$. Quadrant Q1 is the outward interactions, Q2 represents the sweeps, Q3 is the inward interactions, and Q4 is the ejections. Q1 and Q3

represent counter-gradient contributions to the flux ($\overline{u'w'} > 0$), relative to the Reynolds-average profile of $u$ that increases with height, whereas Q2 and Q4 represent the downgradient contributions to the momentum flux.

The contribution of each quadrant $i$ to the momentum flux is quantified as:

$$S_i = \frac{\overline{u'w'}_i}{\overline{u'w'}} \tag{1}$$

where

$$\overline{u'w'}_i = \frac{1}{T_p}\int_0^{T_p} u(t)w(t)I_i dt \tag{2}$$

where $I_i$ is the identity function (1 if $u(t)$ and $w(t)$ are in quadrant $i$). The time fraction $D$ within the time period $T_p$ is:

$$D_i = \frac{1}{T_p}\int_0^{T_p} I_i(t)dt \tag{3}$$

A particular interest here is how the LLJ potentially alters the contribution of sweeps and ejections to the total momentum flux. To assess this, we examine the difference in the contributions of Q4 and Q2 ($\Delta S_0 = S_4 - S_2$).

This difference can be quantified as:

$$\Delta S_0 = \frac{1}{2}R_{uw}\sqrt{2\pi}\left(\frac{1}{3}R_{uw}(M_{03} - M_{30}) + (M_{21} - M_{12})\right) \tag{4}$$

where $R_{uw}$ is the correlation between $u$ and $w$, calculated over the time period $T_p$:

$$R_{uw} = \frac{\overline{u'w'}}{\sigma_u \sigma_w} \tag{5}$$

The dimensionless third-order moments $M_{ij}$ are given by:

$$M_{ij} = \frac{w^i u^j}{\sigma_w^i \sigma_u^j} \tag{6}$$

where the $i$ and $j$ denote the power to which the $w$ and $u$ are raised. The sum of $i$ and $j$ must be equal to three in this case, due to these being the third moments. The third-order moments inform us about the symmetry of the underlying distribution (i.e., the skewness).

### 2.3. Determination of Low-Level Jet

There are several ways to obtain wind profiles and identify the LLJ. Rawinsondes provide in situ measurements of the wind profiles, but operational soundings are typically limited to just twice-daily launches. Wind profiles can be derived from the Next Generation Weather Radar (NEXRAD) by assimilating Doppler velocities over the volume scan after a quality-control algorithm is applied, however the retrieved velocities are sensitive to the choice of assimilation scheme and there are also issues with data availability (e.g., Fast et al., 2008; Newsom et al., 2014). Reanalysis data sets are a common source used to obtain wind profiles to study the LLJ and are appealing given the uninterrupted, dynamically consistent assimilated data from a numerical model and multiple sources of observations.

Several options for reanalysis exist, and the National Centers for Environmental Prediction (NCEP) North American Regional Reanalysis (NARR, Mesinger et al., 2006) is chosen to follow other studies that use NARR to examine the LLJ (Doubler et al., 2015; Hodges & Pu, 2019; Yu et al., 2017). Characteristics of the LLJ (e.g., diurnal fluctuations, mean speed, and mean elevation) are similar between NARR and rawinsonde observations (Berg et al., 2015; Walters et al., 2014), making NARR a viable tool to assess the presence and intensity of a LLJ. NARR uses NCEP's Eta Model with a three-dimensional variational data-assimilation framework that incorporates a diverse set of observations onto a 32-km horizontal grid with 45 vertical levels with data every 25 hPa below 700 hPa. Wind profiles are constructed using the wind on isobaric levels and the 10-m wind. Although a greater number of vertical levels would be helpful, Walters et al. (2014) and Berg et al. (2015) note that NARR is still suitable, but there is an underestimation of the frequency of strong (>20 m $s^{-1}$) LLJs.

In the classic climatological analysis of LLJs by Bonner (1968), a LLJ occurs when there is a speed maximum below 3 km that is greater than 12 m $s^{-1}$ and decreases at least 6 m $s^{-1}$ above the maximum. More recent work (Andreas et al., 2000; Banta et al., 2002; Walters et al., 2008) also advocate that the wind shear below the jet maximum is included to ensure that a local maximum exists. The NARR wind profiles are used to classify the LLJ into four categories of intensity (C0, C1, C2, and C3) based on maximum wind speed below 700 hPa and the vertical wind speed shear, which is the wind speed difference between the maximum wind speed and minimum wind speed above (up to 700 hPa) or below the wind speed maximum.

Most studies follow Bonner's (1968) original classification with only minor modifications. The three categories used to classify the LLJ here are the same as Walters et al. (2008) where C1, C2, and C3 and are defined as jet speeds ≥12 m $s^{-1}$ and vertical shear ≥6 m $s^{-1}$, jet speeds ≥16 m $s^{-1}$ and vertical shear ≥8 m $s^{-1}$, and jet speeds ≥20 m $s^{-1}$ and vertical shear ≥10 m $s^{-1}$, respectively. If no LLJ is present, the profile is categorized as C0. LLJs are also restricted to only southerly LLJ events (i.e., the meridional component must be positive).

## 3. Results and Discussion

### 3.1. General Characteristics Under Different LLJ Criteria

Characteristics of the LLJ classification are shown in Figure 1 and reported in Table 1. In addition to the number of half-hour intervals, the percentage of samples that occurred in each category that also had 100% data in the half-hourly interval with respect to all possible half-hourly intervals is listed. The amount of half-hourly intervals with 100% data in each LLJ bin is 68%, 25%, 22%, and 20%, for C0, C1, C2, and C3, respectively. The maximum speed of the jet is well-correlated with the classification, and the tail toward higher wind speeds of C0 is a result of not meeting the wind shear criteria or if the wind direction is northerly. For stronger wind speeds, the pressure level of the maximum wind speed decreases from 893 to 882 hPa, which is consistent with other climatologies, for example, Song et al. (2005).

The LLJ classification is also slightly related to the air temperature measured at the tower with stronger LLJ classes corresponding to warmer temperatures. This could be related to different synoptic conditions that are related to LLJ formation such as warm air advection or to local impacts such as entrainment of warm layer from aloft. Even though the LLJ is typically decoupled from the surface-layer, greater vertical wind shear associated with a stronger LLJ could increase the surface temperatures through greater entrainment of the warm air aloft. To provide a rough estimate of the relative contribution, the temperature from reanalysis data just above the surface, which is presumably in the residual layer, is an indication of the background temperature. There is a 3 K difference in the background temperature between C0 and C1, while the tower data indicates a 4 K difference. Since a LLJ is typically accompanied by warm air advection from the south, temperature advection explains much of the difference between no-LLJ and LLJ conditions. In contrast, between C1, C2, and C3 the surface temperature increases by about 2 K for each category, but the background temperature increases by <0.5 K for each step of category. This suggests that while some component of the temperature is driven by enhanced warm air advection associated with stronger southerly winds, the other 1.5 K warming for each step of the jet category is likely related to enhanced vertical mixing near the surface.

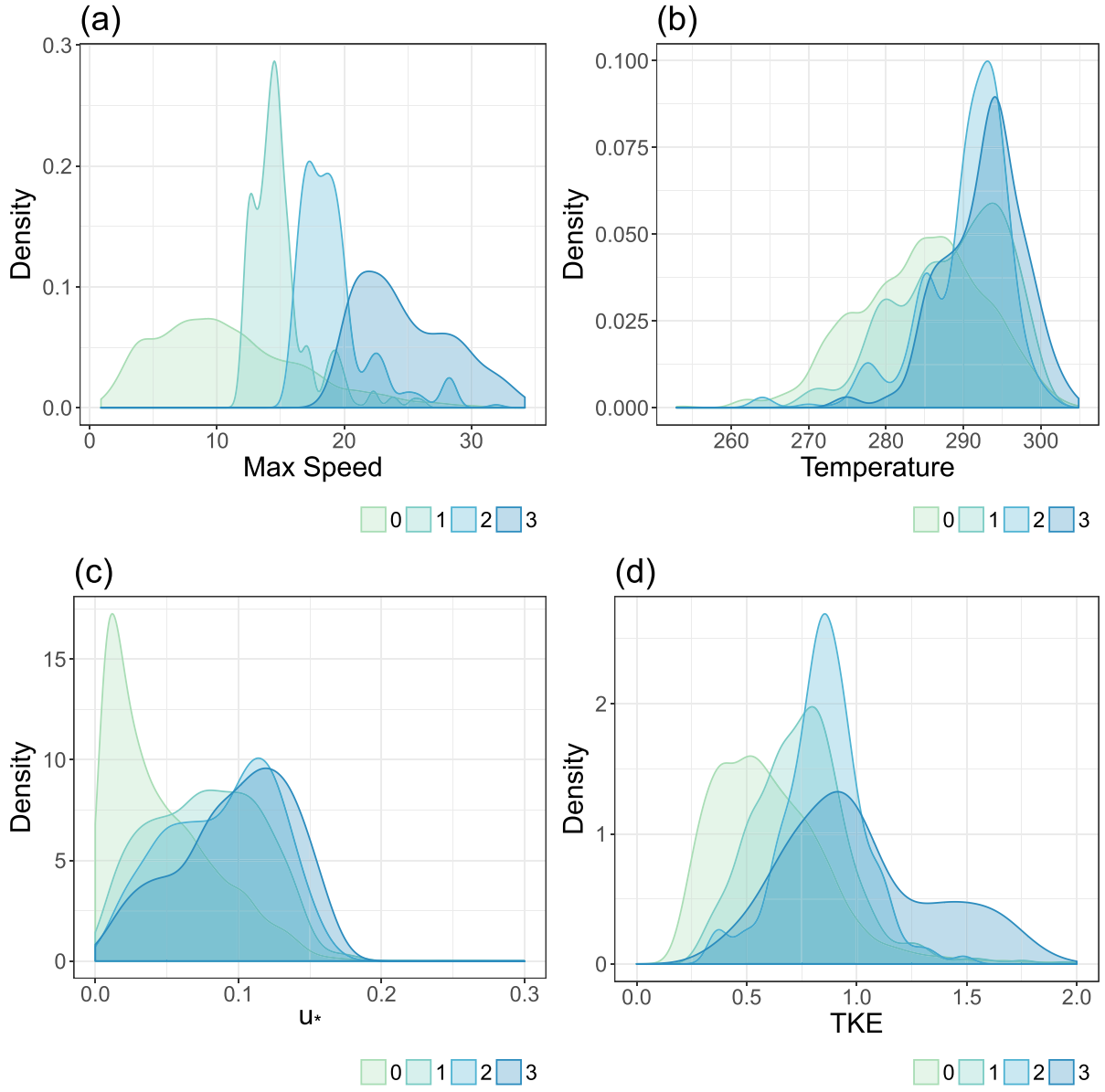


**Figure 1.** Density functions for (a) maximum LLJ velocity (m $s^{-1}$), (b) Temperature [K], (c) friction velocity ($u_*$) (m $s^{-1}$), and (d) turbulent kinetic energy ($m^2 s^{-2}$) for different LLJ criteria classes: no LLJ (C0), weak LLJ (C1), medium LLJ (C2), and high LLJ (C3). LLJ, low-level jet.

**Table 1**
*Mean Values of LLJ and Turbulent Characteristics for Each LLJ Class*

| LLJ | Number of observations | Pressure level of maximum LLJ (hPa) | Max LLJ speed (m $s^{-1}$) | 3-M temperature (K) | $u_*$ (m $s^{-1}$) | z/L | TKE (m $s^{-2}$) | $\sigma_u/u_*$ | $\sigma_v/u_*$ | $\sigma_w/u_*$ | $\sigma_u / \bar{U}$ | $\sigma_v / \bar{U}$ | $\sigma_w / \bar{U}$ |
|---|---|---|---|---|---|---|---|---|---|---|---|---|---|
| C0 | 6181 | – | 10.853 | 284.490 | 0.046 | 3.21 | 0.612 | 24.684 | 21.249 | 9.152 | 0.230 | 0.190 | 0.089 |
| C1 | 529 | 893.0 | 15.029 | 288.676 | 0.078 | 1.56 | 0.767 | 14.403 | 11.850 | 5.981 | 0.195 | 0.156 | 0.088 |
| C2 | 301 | 889.4 | 19.176 | 290.301 | 0.089 | 1.32 | 0.854 | 12.928 | 10.578 | 5.122 | 0.196 | 0.157 | 0.082 |
| C3 | 158 | 882.8 | 24.813 | 292.591 | 0.098 | 1.09 | 1.012 | 13.340 | 11.010 | 5.005 | 0.202 | 0.175 | 0.079 |

Abbreviation: LLJ, low-level jet.

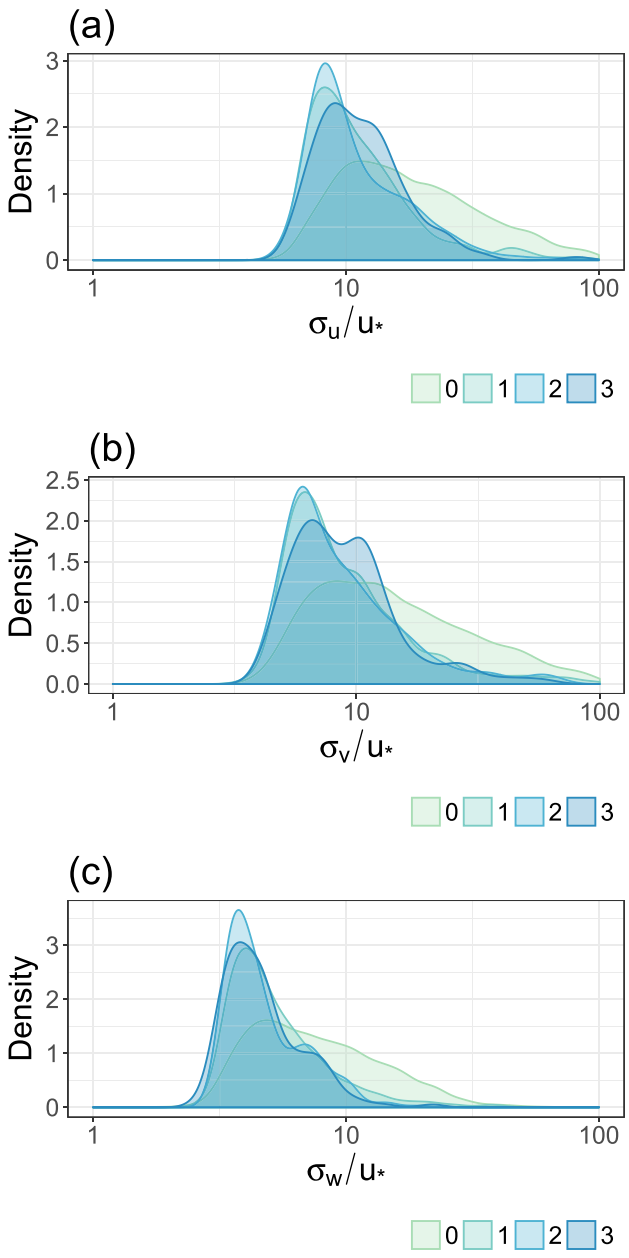


**Figure 2.** Density functions for the normalized velocity standard deviation (a) $\sigma_u/u_*$, (b) $\sigma_v/u_*$, and (c) $\sigma_w/u_*$ wind components for the different LLJ criteria classes. LLJ, low-level jet.

The increased wind speed is also correlated with an increase in the observed friction velocity ($u_*$). This is the first indication that the LLJ does have an impact on surface-layer turbulence characteristics. While the increase in friction velocity would be observed in response to an increase in wind speed, we maintain that this increase is directly due to the LLJ since this is a dominant mechanism for increasing wind speeds aloft and thus impacts the surface-layer properties. The increase in LLJ magnitude also impacts the turbulence kinetic energy (TKE: $0.5(u'^2 + v'^2 + w'^2)$), with the TKE rising from 0.612 $m^2\ s^{-2}$ in non-LLJ case to 1.012 $m^2\ s^{-2}$ in C3. The long tail of large TKE values in C3 is particularly noteworthy.

The velocity standard deviations normalized by the friction velocity $u_*$ are shown in Figure 2. Note that due to the nocturnal turbulence being less well developed than daytime conditions, the $u_*$ values are smaller than corresponding daytime values, resulting in the normalized standard deviations being larger. For each component of the flow, the presence of the LLJ coincided with a reduction of normalized standard deviation of approximately 50% (Table 1). The non-LLJ cases exhibited higher frequencies of larger normalized standard deviations in the tail of the distribution. The non-LLJ cases are generally associated with weaker turbulence and less shear than if an LLJ was present. This lack of turbulence is likely the reason for the higher contributions in the tail of the distribution. The peak $\sigma_w/u_*$ lies at values smaller than $\sigma_u/u_*$ and $\sigma_v/u_*$ and suggests anisotropy in the structure of the turbulent flow. Additionally, $\sigma_u/u_*$ is consistently larger than $\sigma_v/u_*$, again suggesting anisotropic turbulence (recall that the coordinate system is rotated such that $u$ is in the direction of the mean wind). Curiously, the normalized standard deviations were insensitive (invariant) to increasing LLJ strength; the main differences in the statistics were between the absence and the presence of the LLJ. We also computed the dimensionless turbulent intensities ($\sigma_u / \bar{U}$, $\sigma_v / \bar{U}$, and $\sigma_w / \bar{U}$). The differences among these quantities are analogous to the behavior of $\sigma_u/u_*$, $\sigma_v/u_*$, and $\sigma_w/u_*$ above, implying again that the turbulence is anisotropic.

### 3.2. Spectral Analysis Under Different LLJ Criteria

The power spectra for the $u$, $v$, and $w$ wind components as a function of normalized frequency ($fz / \bar{U}$, where $z$ is the measurement height of 3m) are shown in Figure 3 for each LLJ case. For the $u$ spectra, there was a noticeable impact for the intermediate and strong LLJ cases (C2 and C3) in which the power is generally reduced at all frequencies. In the case of the $v$ component, there was an increase in the contribution of the low frequencies in C1–C3 (below approximately 0.1), a shift in the peak contribution to a lower frequency, and a slight reduction in the middle frequencies relative to the non-LLJ case. The $w$-spectra show relatively little variation across the LLJ classifications, with a slight increase in the low frequencies (below 0.2) and little to no change in the mid-frequencies. There is a noticeable drop in the highest frequency contributions in the C2 and C3 cases. While it is unclear exactly what the cause of the high-frequency dropoff is, it may be due to the frequency normalization in these cases. It is unlikely to be an instrumentation issue as these cases are distributed across the time period and interspersed with the other cases that are observed with the same instrument.

The profoundly different shapes of the $u$ and $v$ normalized power spectra may be an indication that the turbulence is anisotropic. Most noticeable is the greater contribution to power at low scales for the $u$

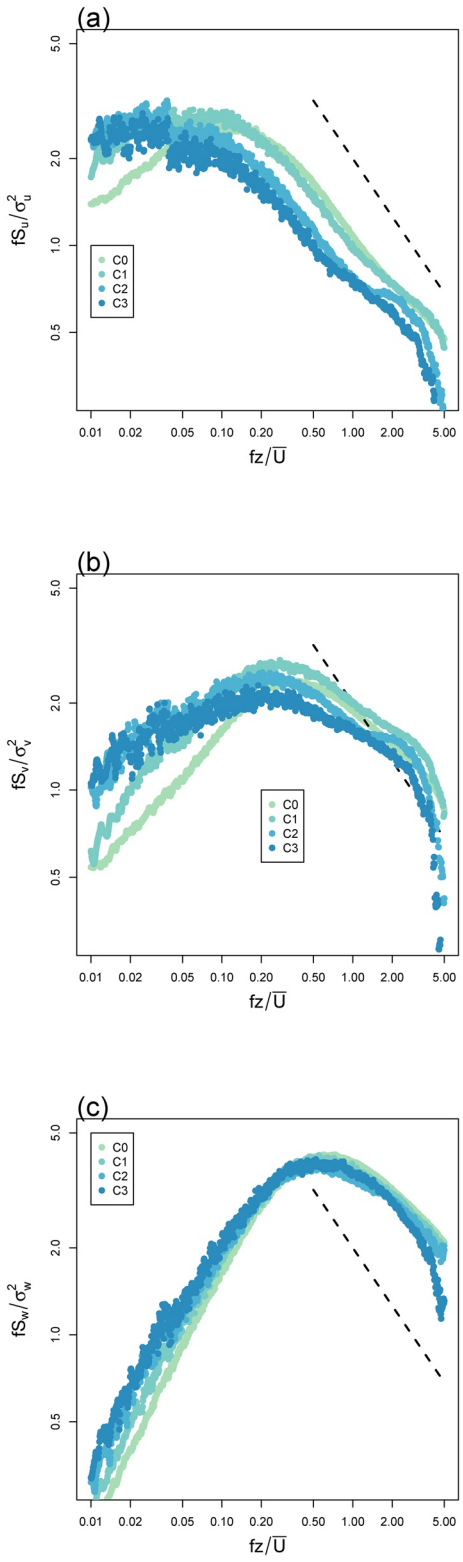


**Figure 3.** Normalized power spectra for (a) $S_u$ / $\sigma_u^2$, (b) $S_v$ / $\sigma_v^2$, and (c) $S_w$ / $\sigma_w^2$ as a function of normalized frequency ($fz$ / $\bar{U}$) for different criteria of low-level jet. Dashed lines show the −2/3 slope for reference.

component, hinting at the importance of mesoscale aspects of the turbulence. The $v$ component contained a greater fraction of its power at smaller scales ranging from 0.5 to 4.0, the reason for which is not obvious. This anisotropy would be consistent with the existence of shear-driven coherent structures (streaks) oriented along the shear-parallel direction (Khanna & Brasseur, 1998; Moeng & Sullivan, 1994). Unlike horizontal convective rolls (Alpers & Brümmer, 1994), buoyancy-generation mechanism are not required to form these streaks. We acknowledge that this explanation is speculative, since anisotropy does not automatically guarantee these streaks are present. Power spectra in the cross-streak ($v$) orientation would presumably contain higher frequency contributions associated with the streak structures, whereas spectra along the streak long axes would be characterized by lower-frequency, mesoscale contributions. The $w$-spectra contain little power at the larger scales and peak at scales roughly corresponding to the depth of the shallow decoupled surface-layer.

In order to further examine the possible role of the anisotropy of the flow and how the LLJ impacts the relative contribution of the wind components, we examined the ratio of the normalized spectra for $S_v$ and $S_w$ relative to the $S_u$ component (Figure 4). In the case of isotropic turbulence this ratio would be expected to be 4/3. For the $v$ component under non-LLJ conditions, the $v$ spectra were generally less than the $u$ component at lower frequencies (<0.5), and the ratio approaches the theoretical 4/3 value in the inertial subrange. This general trend was still observed under the presence of the LLJ. There does not appear to be a systematic alteration of the spectral ratios with increasing strength of the LLJ.

The relative contribution of the $w$ component is shown in Figure 4b. In this case, the same general trend is observed, with little to no variation due to the presence or magnitude of the LLJ. However, in this case we note that the ratio of the $S_w/S_u$ reaches a maximum value of approximately one in the inertial subrange rather than the expected 4/3 value that would be present under isotropic conditions.

### 3.3. Sweep-Ejection Characteristics Under Different LLJ Criteria

The distribution of the correlation $R_{uw}$ for the different LLJ classes is shown in Figure 5a and Table 2. Under no LLJ conditions (C0), there is a bimodal distribution to the correlation factor with peak correlations at 0.2 and −0.26. The positive correlations could potentially be attributed to the lack of shear relative to periods when an LLJ is present (and hence weaker vertical gradient in the mean $U$ in the C0 class). Another possible explanation for the positive $R_{uw}$ could be the weak turbulence during these conditions, resulting in intermittency in the turbulence. This could result in half-hour periods with a few strong eddies moving counter to the gradient and resulting in a positive correlation during these periods. With the presence of the LLJ, almost all of the time periods are exhibiting the expected negative correlations associated with downward momentum transport. The $R_{uw}$ correlation decreases slightly with increasing LLJ case, with mean values of C1: −0.24, C2: −0.21, and C3: −0.19. To better understand how the presence and magnitude of the LLJ impacts the flow beyond the means and correlations, we investigate the sweep and ejection characteristics associated with each LLJ class.

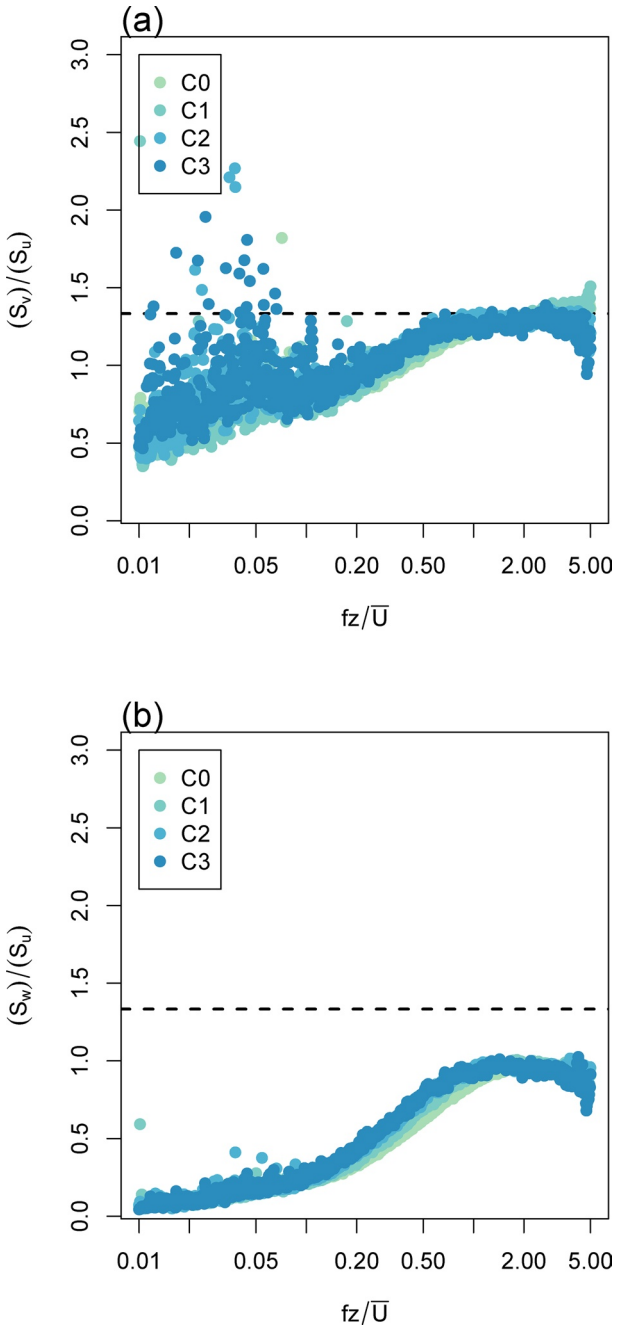


**Figure 4.** Ratio of the (a) $(S_v/S_u)$ power spectra as a function of normalized frequency ($fz$ / $\overline{U}$ and (b) $(S_w/S_u)$ power spectra for different criteria of low-level jet.

Figure 5b shows the difference in the sweeps (Q2) and ejections (Q4), $\Delta S_0$. The data do not show a strong preference for sweeps versus ejections for any of the LLJ classifications. For non-LLJ conditions, there is a small difference of −0.07 (standard deviation: 1.69). With the presence of a LLJ, the mean values for $\Delta S_0$ are all slightly positive. For the C1 case, the difference increases to 0.16 (4.82) indicating a slight dominance by ejections. As the LLJ increases to C2, the difference in contributions from sweeps decreases (mean: 0.024, standard deviation: 0.35). For C3, the difference decreases further to a mean of 0.095 with an increased standard deviation of 0.66.

The alterations of the sweep-ejection characteristics are seen with slight changes to the percentage of time within each quadrant during the half-hour periods (not shown). With the presence of the LLJ, there is a slight increase in the percentage of time in quadrants 2 and 4, with slight decreases in quadrants 1 and 3. The distributions do not change as a function of intensity of the LLJ.

The relative contributions of each quadrant to the total momentum flux during each LLJ class is shown in Figure 6. Recall that S1 and S3 are the contributions from the outward and inward interaction quadrants respectively. These quadrants both represent counter-gradient flow relative to the downward flux of momentum. Quadrants S2 and S4 are the contributions to the flux from sweeps and ejections, respectively. Under non-LLJ conditions, there is a bimodal distribution in each quadrant with relatively equal additions from both positive and negative contributions to the total flux. For weak LLJ conditions, there is a pronounced contribution from the negative (S1 and S3) and positive (S2 and S4) contributions to the flux. With increasing LLJ magnitude, the peak of this relative flux contribution decreases, with the contribution PDFs becoming slightly more dispersed.

The distributions of the third-order moments calculated from Equation 6 are shown in Figure 7. These moments are impacted by both the presence and magnitude of the LLJ. The most significant changes are seen in $M_{03}$ and $M_{12}$, with the mean of both increasing with the strength of the LLJ. For the $M_{03}$, the mean (standard deviation) of each distribution changes from −0.10(14.32) for C0, to 0.20(4.19) for C1, to 0.40(4.92) for C2 and 1.60(3.44) for C3. The $M_{12}$ values are −0.015(0.33), −0.002(0.53), 0.019(0.12), and 0.05(0.32). The small positive values of $M_{30}$ imply a slight preference for stronger, narrow updrafts and weaker, broader downdrafts, although the mean values for the $M_{30}$ and also $M_{21}$ do not vary significantly with LLJ magnitude.

## 4. Conclusions

We have investigated the impact of the presence and intensity of the Great Plains low-level jet on the surface-layer turbulent characteristics using a long-term data set of eddy-covariance observations. We found that the presence of the LLJ alters the distribution of the normalized wind velocity standard deviations and the turbulence intensity. Spectral analysis indicates that the presence of the LLJ leads to substantial differences in the $u$ and $v$ spectra, implying anisotropy that we attribute to possible mesoscale organization in the form of low-level boundary-layer streaks in the along-shear direction (oriented with the mean flow). The $v$-spectra and $w$-spectra also differ substantially, indicating substantial flow anisotropy between vertical and horizontal components. In times where the strongest LLJ are present, there is a noticeable decrease in the high-frequency contributions to

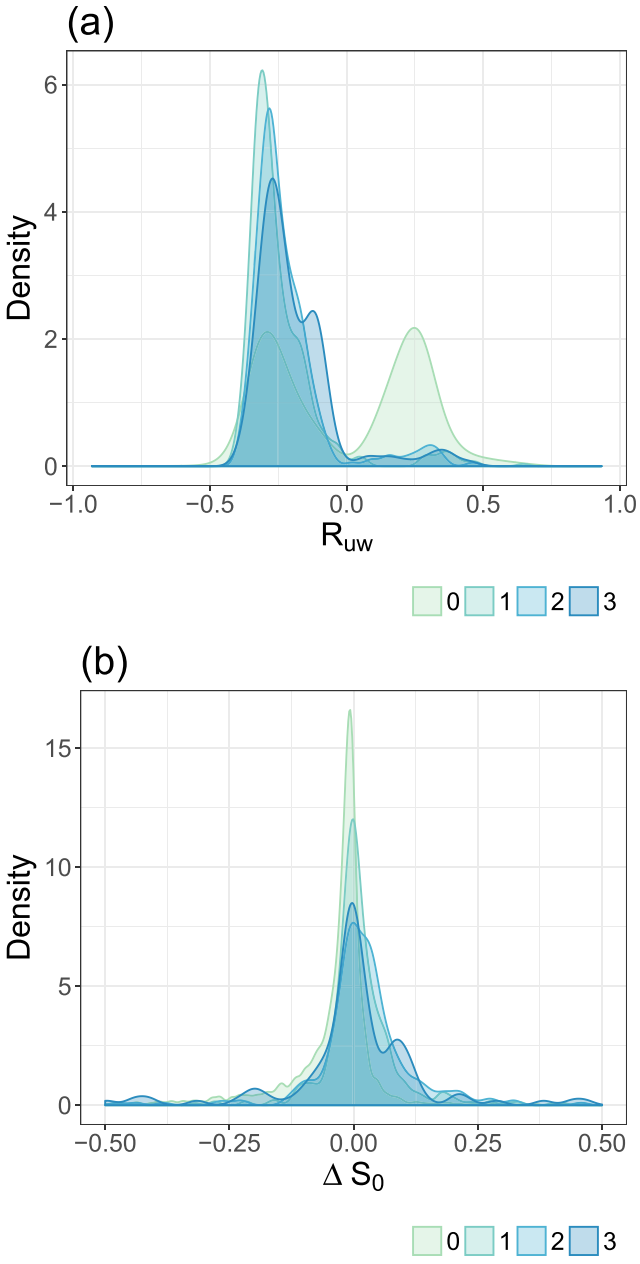


**Figure 5.** Distribution of (a) correlation between $u$ and $w$ and (b) difference in sweeps and ejections as a function of LLJ criteria class. LLJ, low-level jet.

the $w$-spectra. In addition to the LLJ effects on flow isotropy, we found that the LLJ alters the correlation between $u$ and $w$ and the nature of the sweeps and ejections in the surface-layer.

Although the presence of the LLJ alters these characteristics, the intensity of the LLJ appears to have minimal impact. The intensity of the LLJ does impact the distribution of the relative contribution by each quadrant to the flux. With increasing LLJ intensity, the peak of the distribution is decreased and the distribution becomes more dispersed. This behavior is also indicated in increases in the third-order moments $M_{03}$ and $M_{12}$, while the $M_{30}$ and $M_{21}$ moments are not significantly impacted by the intensity of the LLJ.

Our results generally confirm the results from previous studies conducted on shorter time periods. While we see some alteration of the turbulent intensity, we find the dominant impacts to be on the distributions of the flow under conditions when a LLJ is present. Similar to Prabha et al. (2007) and El-Madany et al. (2014), our results demonstrate that the LLJ impacts the spectra, most dominantly at the lower frequencies. The analysis of the sweep and ejection characteristics and the third-order moments show the increasing roles of the both negative and positive contributions of the flux. This implies a strong alteration of the flow, with some of those contributions being counter-gradient similar to Prabha et al. (2007). This alteration of the flow and the role of potential counter-gradient contributions to the flux could be responsible for the trend in the correlation coefficients with increasing LLJ magnitude.

Given our focus on assessing the potential impacts of the presence and magnitude of the LLJ, we do not explicitly account for the role of stability on alteration of the surface-layer statistics. Our determination of the LLJ criteria does take into account changes in the mean wind profile and the criteria also represents changes of the shear profile. These two factors may alter the surface-layer stability observed at the tower. The response of surface-layer turbulence should be primarily influenced by the presence and intensity of the LLJ, but future studies should examine the potential combined effects of changes in the LLJ in relation to changes in surface-layer stability.

Our findings are relevant to broader issues such as surface pollution. Previous studies include Corsmeier et al. (1997) that use a case study during one night to examine a secondary nocturnal ozone maximum related to a LLJ over a rural site in Germany. Hu et al. (2013) also focus on how overnight the ozone can be mixed down from the residual layer into the surface layer by the enhanced shear below the LLJ. Neither study sought to characterize the anisotropy of the turbulence. Using our multiyear data that offered a larger sample of LLJ conditions, we were able to investigate if the LLJ strength impacts the turbulence characteristics over a native tallgrass prairie. Although pollution is typically thought of as an urban concern, annual burning of the prairie in Kansas can produce poor air quality over a large portion of the state (Baker et al., 2016). If a LLJ is present, it greatly impacts the transport and mixing of pollutants.

In conclusion, we note that the presence of the LLJ unequivocally impacts the nature of surface-layer turbulence. While many of these factors are sensitive only to the presence of the LLJ, other factors, such as the correlation and some of the third-order moments are sensitive to both the presence and the intensity of the LLJ.

**Table 2**
*Mean Values of Sweep-Ejection Parameters for Each LLJ Class*

| LLJ | $R_{uw}$ | $\Delta S_0$ | S1 | S2 | S3 | S4 | $M_{03}$ | $M_{30}$ | $M_{21}$ | $M_{12}$ |
|---|---|---|---|---|---|---|---|---|---|---|
| C0 | 0.000 | −0.072 | 0.247 | 0.253 | 0.253 | 0.245 | −0.110 | 0.115 | −0.016 | −0.013 |
| C1 | −0.240 | 0.160 | 0.197 | 0.282 | 0.219 | 0.281 | 0.206 | 0.149 | 0.014 | −0.003 |
| C2 | −0.218 | 0.024 | 0.201 | 0.279 | 0.222 | 0.280 | 0.402 | 0.132 | 0.012 | 0.021 |
| C3 | −0.191 | 0.095 | 0.204 | 0.277 | 0.231 | 0.284 | 1.621 | 0.116 | 0.080 | 0.053 |

*Note*. S1–S4 are the fractional contributions of each quadrant to the total flux.
Abbreviation: LLJ, low-level jet.

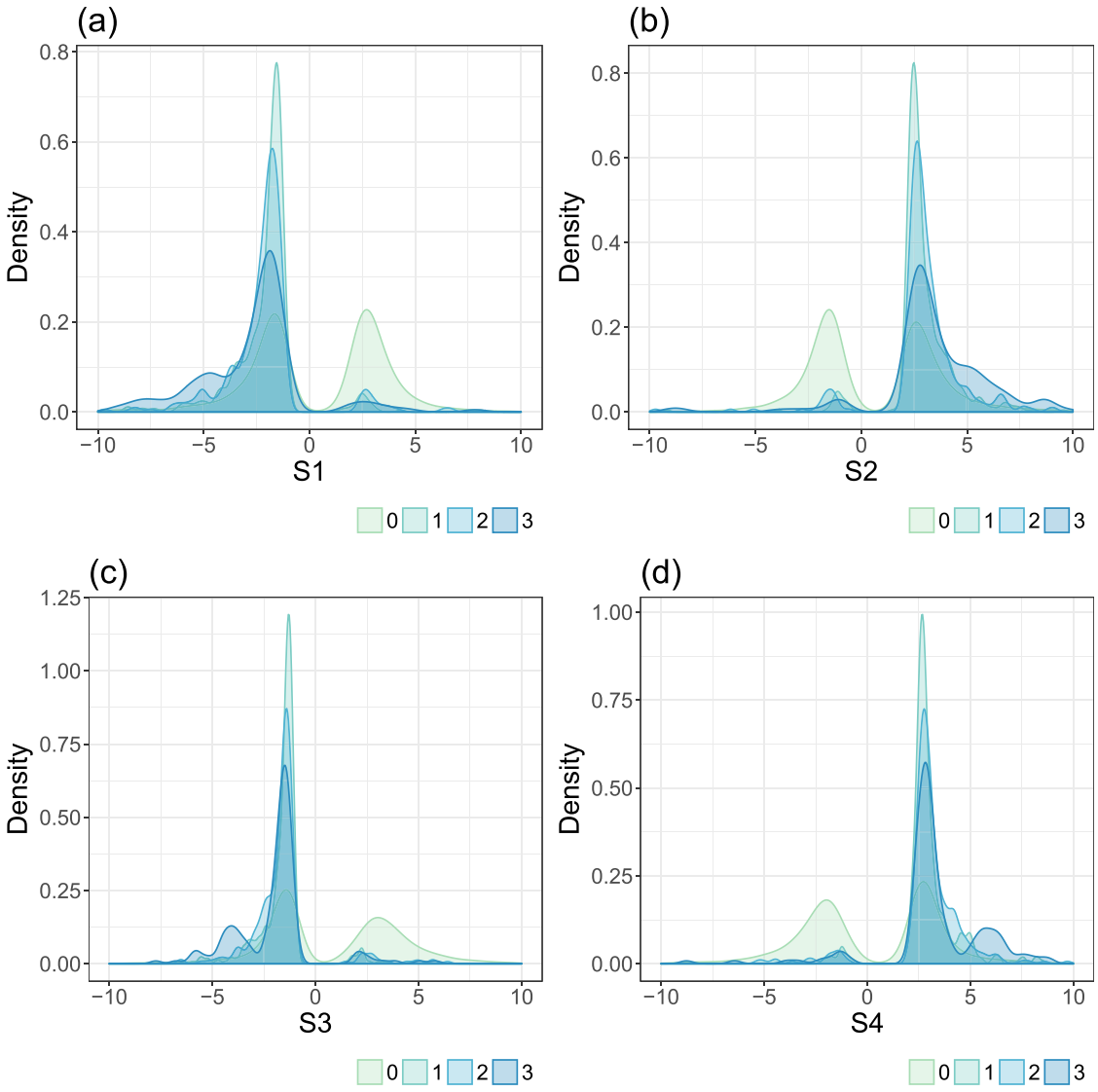


**Figure 6.** Distribution of flux contributions from quadrants 1–4 as a function of LLJ criteria class. LLJ, low-level jet.

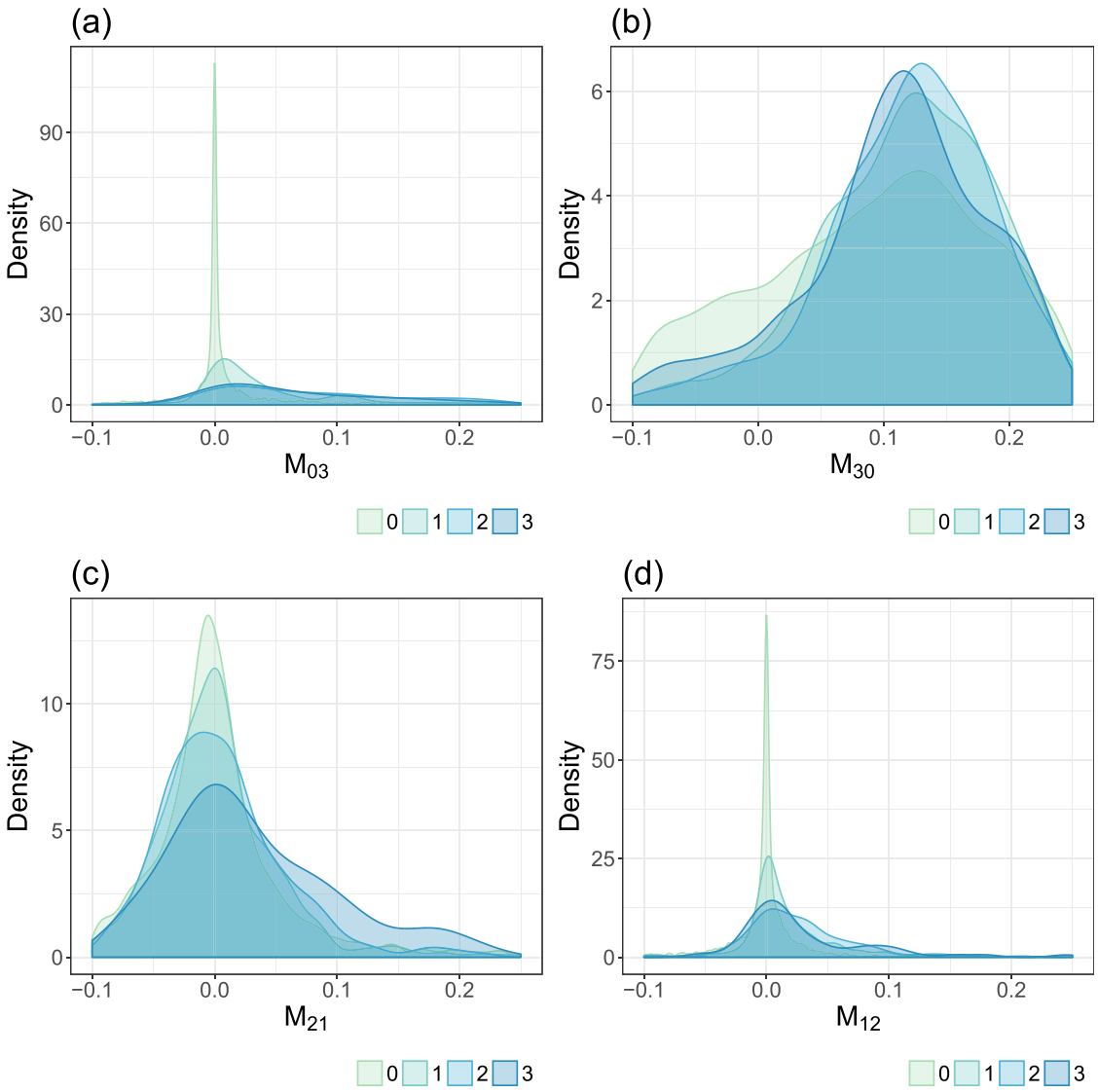


**Figure 7.** Distribution of dimensionless third-order moment terms (a) $M_{03}$, (b) $M_{30}$, (c) $M_{21}$, and (d) $M_{12}$ as a function of LLJ criteria class. LLJ, low-level jet.

## Data Availability Statement

All data presented in this paper are available on the University of Kansas computing system at http://meteo.dept.ku.edu/LLJ_data/

**Acknowledgments**
This work was funded through support from the LTER program at the Konza Prairie Biological Station (DEB-0823341). In addition, the US-KON Ameriflux sites are operated as a portion of the Konza Core Ameriflux Site by N. A. Brunsell sponsored by the US Department of Energy under a sub contract from DE-AC02-05CH11231.

## References

Alpers, W., & Brümmer, B. (1994). Atmospheric boundary layer rolls observed by the synthetic aperture radar aboard the ERS-1 satellite. *Journal of Geophysical Research*, *99*(C6), 12613–12621. https://doi.org/10.1029/94JC00421

Andreas, E. L., Claffy, K. J., & Makshtas, A. P. (2000). Low-level atmospheric jets and inversions over the western Weddell sea. *Boundary-Layer Meteorology*, *97*(3), 459–486. https://doi.org/10.1023/a:1002793831076

Baker, K. R., Woody, M. C., Tonnesen, G. S., Hutzell, W., Pye, H. O. T., Beaver, M. R., et al. (2016). Contribution of regional-scale fire events to ozone and pm2.5 air quality estimated by photochemical modeling approaches. *Atmospheric Environment*, *140*, 539–554. https://doi.org/10.1016/j.atmosenv.2016.06.032

Banta, R. M., Newsom, R. K., Lundquist, J. K., Pichugina, Y. L., Coulter, R. L., & Mahrt, L. (2002). Nocturnal low-level jet characteristics over Kansas during cases-99. *Boundary-Layer Meteorology*, *105*(2), 221–252. https://doi.org/10.1023/a:1019992330866

Berg, L. K., Riihimaki, L. D., Qian, Y., Yan, H., & Huang, M. (2015). The low-level jet over the southern great plains determined from observations and reanalyzes and its impact on moisture transport. *Journal of Climate*, *28*(17), 6682–6706. https://doi.org/10.1175/jcli-d-14-00719.1

Blackadar, A. K. (1957). Boundary layer wind maxima and their significance for the growth of nocturnal inversions. *Bulletin of the American Meteorological Society*, *38*(5), 283–290. https://doi.org/10.1175/1520-0477-38.5.283

Bonner, W. D. (1968). Climatology of the low level jet. *Monthly Weather Review*, *96*(12), 833–850. https://doi.org/10.1175/1520-0493(1968)096⟨0833:COTLLJ⟩2.0.CO;2

Bonner, W. D., & Paegle, J. (1970). Diurnal variations in boundary layer winds over the south-central united states in summer. *Monthly Weather Review*, *98*(10), 735–744. https://doi.org/10.1175/1520-0493(1970)098⟨0735:DVIBLW⟩2.3.CO;2

Brunsell, N. A., Nippert, J. B., & Buck, T. L. (2014). Impacts of seasonality and surface heterogeneity on water-use efficiency in mesic grasslands. *Ecohydrology*, *7*, 1223–1233

Cook, K. H., Vizy, E. K., Launer, Z. S., & Patricola, C. M. (2008). Springtime intensification of the great plains low-level jet and midwest precipitation in GCM simulations of the twenty-first century. *Journal of Climate*, *21*(23), 6321–6340. https://doi.org/10.1175/2008JCLI2355.1

Corsmeier, U., Kalthoff, N., Kolle, O., Kotzian, M., & Fiedler, F. (1997). Ozone concentration jump in the stable nocturnal boundary layer during a LLJ-event. *Atmospheric Environment*, *31*(13), 1977–1989. https://doi.org/10.1016/s1352-2310(96)00358-5

Doubler, D. L., Winkler, J. A., Bian, X., Walters, C. K., & Zhong, S. (2015). An narr-derived climatology of southerly and northerly low-level jets over north America and coastal environs. *Journal of Applied Meteorology and Climatology*, *54*(7), 1596–1619. https://doi.org/10.1175/jamc-d-14-0311.1

Duarte, H. F., Leclerc, M. Y., Zhang, G., Durden, D., Kurzeja, R., Parker, M., & Werth, D. (2015). Impact of nocturnal low-level jets on near-surface turbulence kinetic energy. *Boundary-Layer Meteorology*, *156*(3), 349–370. https://doi.org/10.1007/s10546-015-0030-z

El-Madany, T. S., Duarte, H. F., Durden, D. J., Paas, B., Deventer, M. J., Juang, J.-Y., et al. (2014). Low-level jets and above-canopy drainage as causes of turbulent exchange in the nocturnal boundary layer. *Biogeosciences*, *11*(16), 4507–4519. https://doi.org/10.5194/bg-11-4507-2014

Fast, J. D., Newsom, R. K., Allwine, K. J., Xu, Q., Zhang, P., Copeland, J., & Sun, J. (2008). An evaluation of two nexrad wind retrieval methodologies and their use in atmospheric dispersion models. *Journal of Applied Meteorology and Climatology*, *47*(9), 2351–2371. https://doi.org/10.1175/2008jamc1853.1

Gebauer, J. G., & Shapiro, A. (2019). Clarifying the baroclinic contribution to the great plains low-level jet frequency maximum. *Monthly Weather Review*, *147*(9), 3481–3493. https://doi.org/10.1175/MWR-D-19-0024.1

Helfand, H. M., & Schubert, S. D. (1995). Climatology of the simulated great plains low-level jet and its contribution to the continental moisture budget of the united states. *Journal of Climate*, *8*(4), 784–806. https://doi.org/10.1175/1520-0442(1995)008<0784:COTSGP>2.0.CO;2

Higgins, R. W., Yao, Y., Yarosh, E. S., Janowiak, J. E., & Mo, K. C. (1997). Influence of the great plains low-level jet on summertime precipitation and moisture transport over the central united states. *Journal of Climate*, *10*(3), 481–507. https://doi.org/10.1175/1520-0442(1997)010⟨0481:IOTGPL⟩2.0.CO;2

Hodges, D., & Pu, Z. (2019). Characteristics and variations of low-level jets and environmental factors associated with summer precipitation extremes over the great plains. *Journal of Climate*, *32*(16), 5123–5144. https://doi.org/10.1175/jcli-d-18-0553.1

Hoecker, W. H. (1963). Three southerly low-level jet systems delineated by the weather bureau special pibal network of 1961. *Monthly Weather Review*, *91*(10), 573–582. https://doi.org/10.1175/1520-0493(1963)091⟨0573:TSLJSD⟩2.3.CO;2

Holton, J. R. (1967). The diurnal boundary layer wind oscillation above sloping terrain. *Tellus*, *19*(2), 200–205. https://doi.org/10.3402/tellusa.v19i2.9766

Hu, X.-M., Klein, P. M., Xue, M., Zhang, F., Doughty, D. C., Forkel, R., et al. (2013). Impact of the vertical mixing induced by low-level jets on boundary layer ozone concentration. *Atmospheric Environment*, *70*, 123–130. https://doi.org/10.1016/j.atmosenv.2012.12.046

Jahn, D. E., & Gallus, W. A. (2018). Impacts of modifications to a local planetary boundary layer scheme on forecasts of the great plains low-level jet environment. *Weather and Forecasting*, *33*(5), 1109–1120. https://doi.org/10.1175/WAF-D-18-0036.1

Kaimal, J. C., & Finnigan, J. J. (1994). *Atmospheric boundary layer flows: Their structure and measurement*. Oxford, UK: Oxford University Press.

Karipot, A., Leclerc, M. Y., Zhang, G., Lewin, K. F., Nagy, J., Hendrey, G. R., & Starr, G. (2008). Influence of nocturnal low-level jet on turbulence structure and CO2 flux measurements over a forest canopy. *Journal of Geophysical Research*, *113*, D10102. https://doi.org/10.1029/2007JD009149

Katul, G., Kuhn, G., Schieldge, J., & Hsieh, C.-I. (1997). The ejection-sweep character of scalar fluxes in the unstable surface layer. *Boundary-Layer Meteorology*, *83*(1), 1–26. https://doi.org/10.1023/a:1000293516830

Khanna, S., & Brasseur, J. G. (1998). Three-dimensional buoyancy- and shear-induced local structure of the atmospheric boundary layer. *Journal of the Atmospheric Sciences*, *55*, 710–743. https://doi.org/10.1175/1520-0469(1998)055<0710:TDBASI>2.0.CO;2

Logan, K. E., & Brunsell, N. A. (2015). Influence of drought on growing season carbon and water cycling with changing land cover. *Agricultural and Forest Meteorology*, *213*, 217–225. https://doi.org/10.1016/j.agrformet.2015.07.002

Mesinger, F., DiMego, G., Kalnay, E., Mitchell, K., Shafran, P. C., Ebisuzaki, W., et al. (2006). North american regional reanalysis. *Bulletin of the American Meteorological Society*, *87*(3), 343–360. https://doi.org/10.1175/BAMS-87-3-343

Mitchell, M. J., Arritt, R. W., & Labas, K. (1995). A climatology of the warm season great plains low-level jet using wind profiler observations. *Weather Forecasting*, *10*(3), 576–591. https://doi.org/10.1175/1520-0434(1995)010⟨0576:ACOTWS⟩2.0.CO;2

Moeng, C.-H., & Sullivan, P. P. (1994). A comparison of shear- and buoyancy-driven planetary boundary layer flows. *Journal of the Atmospheric Sciences*, *51*, 999–1022. https://doi.org/10.1175/1520-0469(1994)051<0999:ACOSAB>2.0.CO;2

Newsom, R. K., Berg, L. K., Pekour, M., Fast, J., Xu, Q., Zhang, P., et al. (2014). Evaluation of single-doppler radar wind retrievals in flat and complex terrain. *Journal of Applied Meteorology and Climatology*, *53*(8), 1920–1931. https://doi.org/10.1175/jamc-d-13-0297.1

Parish, T. R., & Clark, R. D. (2017). On the initiation of the 20 June 2015 great plains low-level jet. *Journal of Applied Meteorology and Climatology*, *56*(7), 1883–1895. https://doi.org/10.1175/JAMC-D-16-0187.1

Parish, T. R., & Oolman, L. D. (2010). On the role of sloping terrain in the forcing of the great plains low-level jet. *Journal of the Atmospheric Sciences*, *67*(8), 2690–2699. https://doi.org/10.1175/2010JAS3368.1

Prabha, T. V., Leclerc, M. Y., Karipot, A., & Hollinger, D. Y. (2007). Low-frequency effects on eddy covariance fluxes under the influence of a low-level jet. *Journal of Applied Meteorology and Climatology*, *46*(3), 338–352. https://doi.org/10.1175/jam2461.1

Shibuya, R., Sato, K., & Nakanishi, M. (2014). Diurnal wind cycles forcing inertial oscillations: A latitude-dependent resonance phenomenon. *Journal of the Atmospheric Sciences*, *71*(2), 767–781. https://doi.org/10.1175/JAS-D-13-0124.1

Smith, E. N., Gebauer, J. G., Klein, P. M., Fedorovich, E., & Gibbs, J. A. (2019). The great plains low-level jet during pecan: Observed and simulated characteristics. *Monthly Weather Review*, *147*(6), 1845–1869. https://doi.org/10.1175/MWR-D-18-0293.1

Song, J., Liao, K., Coulter, R. L., & Lesht, B. M. (2005). Climatology of the low-level jet at the southern great plains atmospheric boundary layer experiments site. *Journal of Applied Meteorology*, *44*(10), 1593–1606. https://doi.org/10.1175/JAM2294.1

Tuttle, J. D., & Davis, C. A. (2006). Corridors of warm season precipitation in the central united states. *Monthly Weather Review*, *134*(9), 2297–2317. https://doi.org/10.1175/MWR3188.1

Uccellini, L. W. (1980). On the role of upper tropospheric jet streaks and leeside cyclogenesis in the development of low-level jets in the great plains. *Monthly Weather Review*, *108*(10), 1689–1696. https://doi.org/10.1175/1520-0493(1980)108⟨1689:OTROUT⟩2.0.CO;210.1175/1520-0493(1980)108<1689:OTROUT>2.0.CO;2

Walters, C. K., Winkler, J. A., Husseini, S., Keeling, R., Nikolic, J., & Zhong, S. (2014). Low-level jets in the North American regional reanalysis (NARR): A comparison with Rawinsonde observations. *Journal of Applied Meteorology and Climatology*, *53*(9), 2093–2113. https://doi.org/10.1175/JAMC-D-13-0364.1

Walters, C. K., Winkler, J. A., Shadbolt, R. P., van Ravensway, J., & Bierly, G. D. (2008). A long-term climatology of southerly and northerly low-level jets for the central united states. *Annals of the Association of American Geographers*, *98*(3), 521–552. https://doi.org/10.1080/00045600802046387

Yu, L., Zhong, S., Winkler, J. A., Doubler, D. L., Bian, X., & Walters, C. K. (2017). The inter-annual variability of southerly low-level jets in north america. *International Journal of Climatology*, *37*(1), 343–357. https://doi.org/10.1002/joc.4708

Zhang, X., Yang, C., & Li, S. (2019). Influence of the heights of low-level jets on power and aerodynamic loads of a horizontal axis wind turbine rotor. *Atmosphere*, *10*(3), 132. https://doi.org/10.3390/atmos10030132

Zhong, S., Fast, J. D., & Bian, X. (1996). A case study of the great plains low-level jet using wind profiler network data and a high-resolution mesoscale model. *Monthly Weather Review*, *124*(5), 785–806. https://doi.org/10.1175/1520-0493(1996)124⟨0785:ACSOTG⟩2.0.CO;2